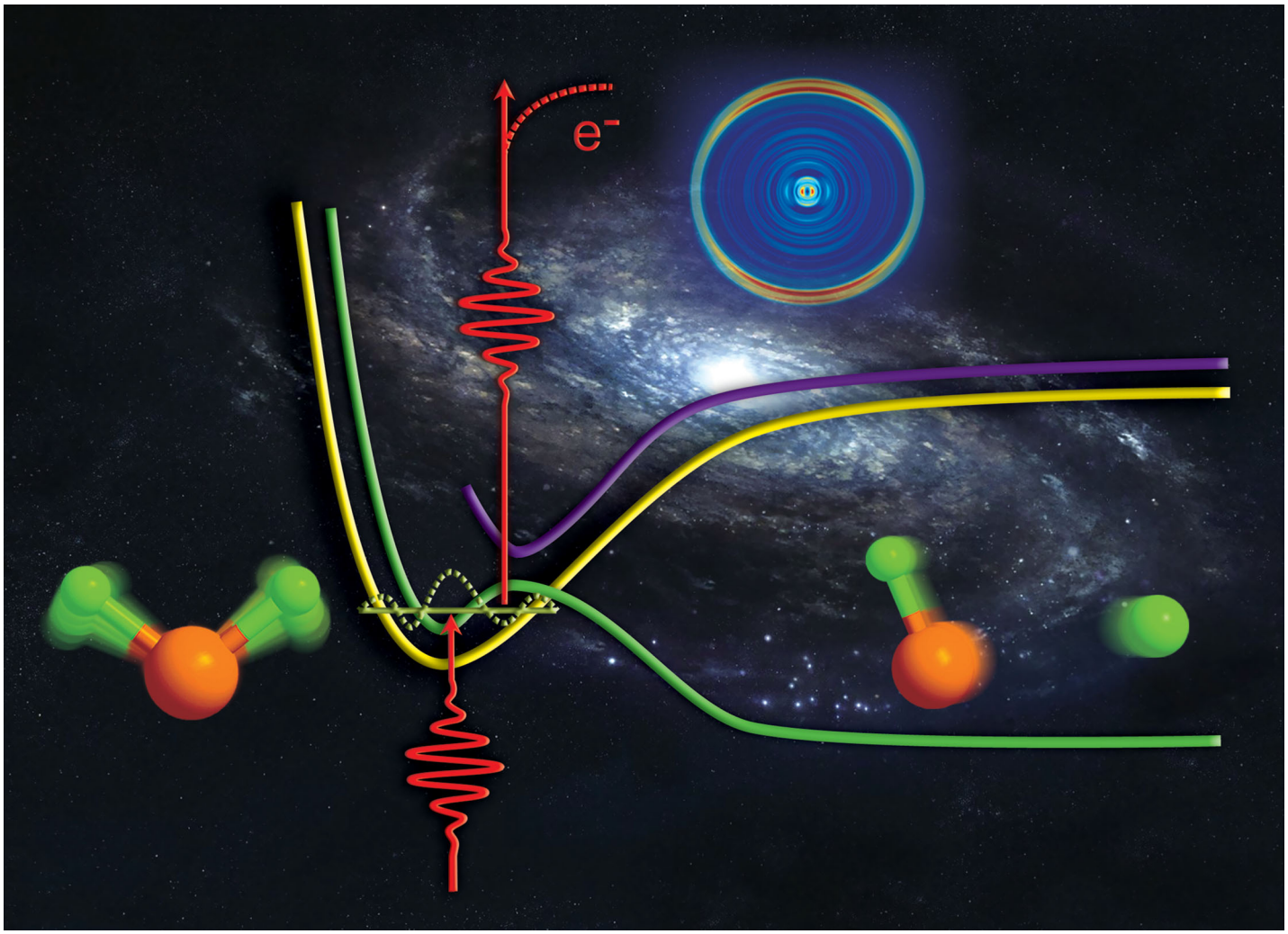

Showcasing research from the Group of Prof. Guorong Wu at the Dalian Institute of Chemical Physics, Chinese Academy of Sciences, China

An accidental resonance mediated predissociation pathway of water molecules excited to the electronic $\tilde{C}$ state

This paper reports the predissociation dynamics of water molecules in the electronic $\tilde{C}$ state, studied using the femtosecond time-resolved photoelectron imaging method. The vibrational excitation effects on the predissociation dynamics of the $\tilde{C}$ state are investigated in detail. An accidental resonance mediated predissociation pathway for the first bending mode excited state in the $\tilde{C}$ state of H_2O is revealed, adding new insights into this important model system for photochemical dynamics.

As featured in:

See Guorong Wu, Xueming Yang *et al.*, *Phys. Chem. Chem. Phys.*, 2017, **19**, 29795.

ROYAL SOCIETY OF CHEMISTRY

rsc.li/pccp

Registered charity number: 207890

PCCP

PAPER

View Article Online
View Journal | View Issue

Cite this: *Phys. Chem. Chem. Phys.*, 2017, **19**, 29795

An accidental resonance mediated predissociation pathway of water molecules excited to the electronic C̃ state†

Zhigang He,‡[a] Dongyuan Yang,‡[ab] Zhichao Chen,[a] Kaijun Yuan,[a] Dongxu Dai,[ac] Guorong Wu*[ac] and Xueming Yang*[ac]

Received 14th September 2017,
Accepted 18th October 2017

DOI: 10.1039/c7cp06286a

rsc.li/pccp

The predissociation dynamics of water molecules in the electronic C̃ state were studied using the time-resolved photoelectron imaging method. Both vibrationless and vibrationally excited states in the C̃ electronic state were studied, with an emphasis on the vibrational excitation effects on the predissociation dynamics of the C̃ state. Besides the well-known rotationally and non-rotationally mediated predissociation pathways (*Proc. Natl. Acad. Sci. U. S. A.*, 2008, **105**, 19148), an accidental resonance mediated predissociation pathway for the first bending mode excited state in the C̃ electronic state of H_2O is revealed, providing an excellent example of competition between non-adiabatic decay pathways involving at least five electronic states.

Introduction

Non-adiabatic processes occur throughout chemistry when electronically excited states are involved. These processes are key to our understanding of important processes in vision chemistry, atmospheric chemistry, interstellar chemistry, *etc.*[1–3] Photochemistry of water in the gas phase has served as a model polyatomic system for the understanding of non-adiabatic dynamics induced by the coupling between different potential energy surfaces. In the last thirty years, numerous experimental and theoretical studies have been devoted to this system from which many details of photochemical and photophysical processes of water molecules in electronically excited states, especially the four lowest singlet states, have been revealed.[4] Among these states, the C̃ state is bound adiabatically with a fully resolved rotational structure, but subject to weak predissociation.[5–10] Photodissociation of water in the C̃ state shows rotational-state dependent predissociation dynamics: for $\langle \hat{J}_a^2 = 0 \rangle$ rotational levels ($\langle \hat{J}_a^2 \rangle$ is the expectation value of the square of the rotational angular momentum about the molecular a-axis), the C̃ state predissociates exclusively through the Ã state *via* electronic coupling and vibrationally hot and rotationally cold ground state $OH(X^2\Pi)$ products are produced; while for $\langle \hat{J}_a^2 \geq 1 \rangle$ rotational states, another channel opens through Coriolis-type coupling to the B̃ surface, generating extremely rotationally hot and vibrationally cold ground state $OH(X^2\Pi)$ products, as well as rotationally hot electronically excited state $OH(\tilde{A}^2\Sigma^+)$ products. Accordingly, the C̃ state shows a lifetime with a clear dependence on $\langle \hat{J}_a^2 \rangle$: with an increase of $\langle \hat{J}_a^2 \rangle$, the lifetime of the C̃ state rapidly decreases.

The relatively long lifetime and ro-vibrationally resolved absorption band of the C̃ state provide a good opportunity for vibrational state-selective excitation of this state and therefore investigation of the vibrational excitation effects on the predissociation dynamics of water in the C̃ state. However, this has not been studied as thoroughly to date. In this paper, we present an experimental study of the predissociation dynamics of water molecules in the C̃ state using the time-resolved photoelectron imaging (TRPEI) technique. Both vibrationless and vibrationally excited states in the C̃ electronic state of H_2O and D_2O are studied to investigate the vibrational excitation effects on the predissociation dynamics of the C̃ state. All vibrationally excited states show a moderate enhancement on the predissociation rate of the C̃ state, except for the first bending mode excited state in the C̃ state of H_2O which shows an "abnormal" high enhancement in the predissociation rate of the C̃ state. Further analysis reveals that this is due to an accidental resonance mediated pathway through the D̃ state, suggesting a new decay mechanism of the C̃ state of H_2O.

[a] *State Key Laboratory of Molecular Reaction Dynamics, Dalian Institute of Chemical Physics, 457 Zhongshan Road, Dalian 116023, Liaoning, China. E-mail: wugr@dicp.ac.cn, xmyang@dicp.ac.cn*
[b] *University of Chinese Academy of Sciences, Beijing 100049, China*
[c] *Synergetic Innovation Center of Quantum Information & Quantum Physics, University of Science and Technology of China, Hefei, Anhui 230026, China*

† Electronic supplementary information (ESI) available: Analysis of the 0.3 eV feature in the TRPES data and the comparison of the photoelectron kinetic energy distributions of the C̃ state with different vibrational excitations. See DOI: 10.1039/c7cp06286a

‡ These authors contributed equally.

Experimental

The experiment was carried out on a velocity map imaging (VMI) spectrometer, constructed recently in our lab and detailed elsewhere.[11] Four different pump wavelengths were used: 248.0 nm (~3.5 μJ), 244.2 nm (~3.1 μJ), 240.1 nm (~2.5 μJ) and 239.0 nm (~2.5 μJ). The bandwidth of the pump pulses was about 400 cm^{-1}. The probe wavelength was fixed at 332.9 nm (6.2–6.7 μJ). Femtosecond laser pulses were obtained from a fully integrated Ti:Sapphire oscillator/regenerative amplifier system (<50 fs, 800 nm, 3.8 mJ and 1 kHz, Coherent, Libra-HE). Two optical parametric amplifiers (OPA, Coherent, OperA Solo), each pumped by a fraction of the fundamental (1.3 mJ per pulse), were used to generate the pump and probe pulses, respectively. UV pulses were combined collinearly on a dichroic mirror without further compression, and then focused using an f/75 lens to intersect a seeded water molecular beam in the interaction region of the VMI spectrometer. Time delays between pump and probe pulses were scanned using a computer-controlled stepper motor which was located upstream of one of the OPAs to change the delay of the input fundamental. The H_2O and D_2O molecular beams were generated by bubbling He of 2.5 bar through the H_2O or D_2O sample at room temperature using a pulsed valve (General Valve) operated at 50 Hz. The pump pulse excited the water molecules from their ground state into a vibrational level of the $\tilde{C}$ state by two-photon absorption whereupon the delayed probe pulse produced photoelectrons *via* one-photon ionization (Fig. 1). Photoelectron images arising from the pump or the probe laser alone were also recorded. The sum of the single color photoelectron images were subtracted in order to correct for background photoelectrons generated from single color multiphoton ionizations. Pump–probe time delays were scanned back and forth multiple times to minimize any small hysteresis effects, and effects caused by the fluctuations and drifts in the laser pulse energies, pointing and molecular beam intensity, *etc.* The 2D photoelectron images were transferred to the 3D distribution using the basis-set expansion method.[12] The time-dependent photoelectron 3D distributions were further integrated along the recoiling angle to derive the kinetic energy distributions of the photoelectron, *i.e.*, time-resolved photoelectron spectra (TRPES). Electron kinetic energy calibration was achieved using multi-photon ionization of Xe atoms. This also served to measure the cross-correlation (*i.e.*, instrumental response function) between the pump and the probe laser pulses. The time-zero overlap was checked before and after the TRPEI measurement of the water molecules. The delay-dependent curve of the electron yield was fitted, based on the approximation that both pump and probe laser pulses have a Gaussian profile. It has to be noted here that only photoelectrons generated by absorption of two pump photons and a single probe photon were taken into account in this analysis, thanks to the capability of the VMI technique in differentially analyzing the outgoing photoelectron as a function of delay with respect to kinetic energy. The derived cross-correlations are summarized in Table 1. The error bars of the cross-correlation represent one standard deviation derived from the fit of the total electron yield to a Gaussian distribution.

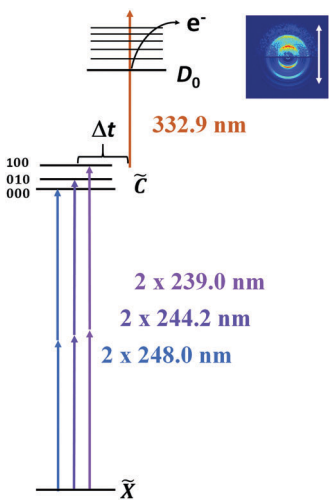

Fig. 1 Schematic view of the pump and probe schemes used in the present experiment.

Table 1 2D globally fitted time constants from the TRPES data. The pump laser wavelengths used, the corresponding vibronic states excited,[5,13–16] and the corresponding cross-correlations are also indicated

	H_2O		D_2O		
λ (nm)	Vibronic state	Lifetime	Vibronic state	Lifetime (ps)	Cross-correlation (fs)
248.0	$\tilde{C}(000)$	1.42 ± 0.15 ps	$\tilde{C}(000)$	5.76 ± 0.35	
244.2	$\tilde{C}(010)$	327^{+23}_{-47} fs	$\tilde{C}(010)$	4.0 ± 0.4	173 ± 7 (H_2O)
					155 ± 4 (D_2O)
240.1			$\tilde{C}(100)$	3.6 ± 0.1	149 ± 14
239.0	$\tilde{C}(100)$	643^{+160}_{-183} fs			153 ± 13

Results and discussion

The experimental results and data analysis

Water molecules were excited into the $\tilde{C}$ state by two-photon absorption whereupon another delayed laser pulse probed the excited state water molecules *via* one-photon ionization (Fig. 1). By tuning the pump wavelength, three different vibrational states of the $\tilde{C}$ electronic state, $\tilde{C}(000)$, $\tilde{C}(010)$ and $\tilde{C}(100)$, were excited. (Vibronic states are denoted by $(\nu_1\nu_2\nu_3)$, where ν_1, ν_2 and ν_3 specify the quantum numbers in the symmetric stretching, bending and asymmetric stretching modes, respectively.) Fig. 2(a)–(c) show the TRPES data of H_2O at pump wavelengths of 248.0, 244.2 and 239.0 nm, respectively. At 248.0 nm, the TRPES data is dominated by a single sharp peak centered at 1.1 eV. The delay dependence of this peak seems to show a simple exponential decay with a lifetime of the order of magnitude of 1 ps. At 244.2 nm, the TRPES data is composed of a strong, sharp peak at around 1.25 eV showing a very fast decay and a weak feature peaked at 1.1 eV with a relatively slow decay dynamics. A feature at 0.3 eV is also presented in this TRPES data and that at 239.0 nm and some of those for D_2O (see Fig. 3(b) and (c)). During the time delay implemented in

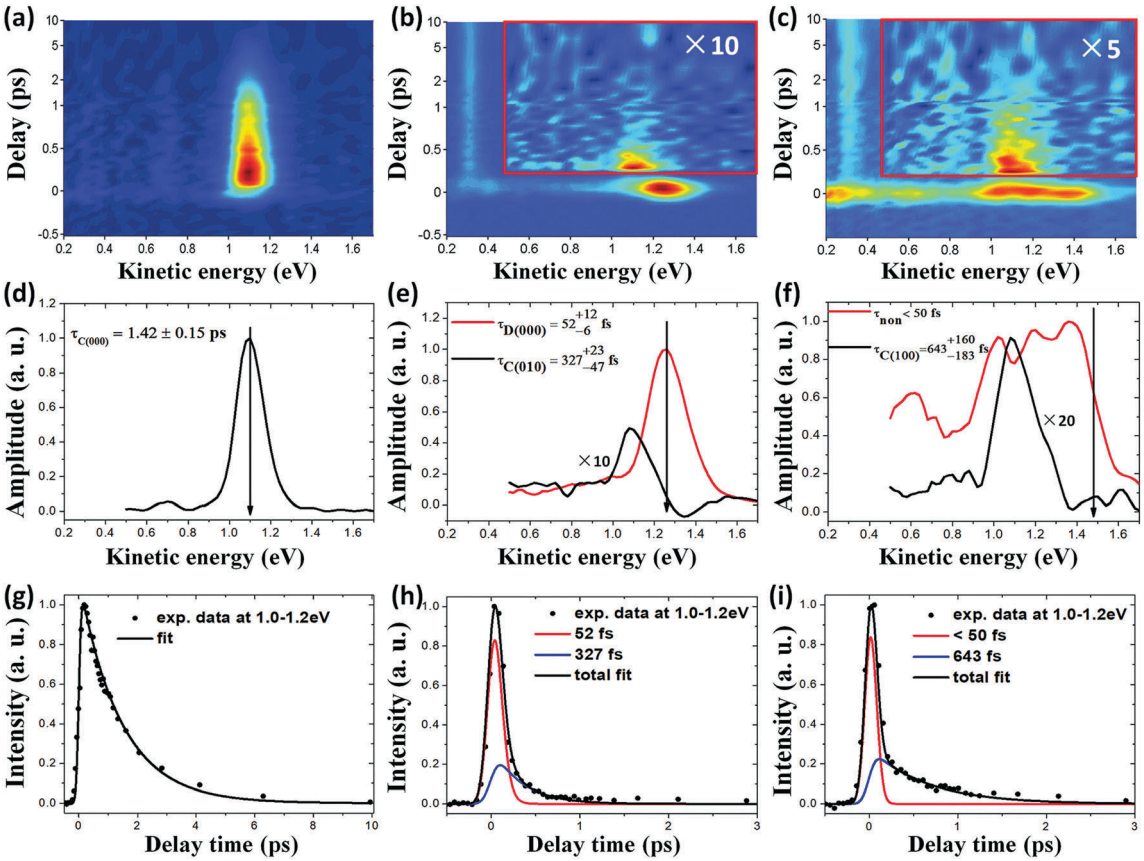

Fig. 2 TRPES of H_2O at pump wavelengths of 248.0 (a), 244.2 (b) and 239.0 nm (c), after subtracting background photoelectrons generated from single color multiphoton ionization. Note that a combination of linear and logarithmic scales is used in the ordinate. (d–f) The photoelectron kinetic energy distributions derived from a 2D global least-squares fit to the data shown in (a–c), respectively. The energetic limit to the ground state of the cation is indicated by the black arrow. (g–i) The delay dependent photoelectron signal integrated over the kinetic energy range 1.0–1.2 eV where the main feature of the $\tilde{C}$ state is located. The transients from the 2D global least-squares fit are also included.

these measurements, no decay of this feature was observed. The TRPES data at 239.0 nm is similar to that at 244.2 nm, except that the fast decaying component becomes very diffuse over the kinetic energy range from 0.2 to 1.5 eV.

In order to extract more detailed information from these TRPES data, a 2D global least-squares method was employed to simultaneously fit data at all time delays and photoelectron kinetic energies. Only photoelectrons with kinetic energies $\geq$0.5 eV were included in order to avoid the interference from the 0.3 eV feature which was found to be associated with the H atom (detailed in the ESI†). The kinetic model used to fit the TRPES data is the same as that used in our previous studies and will not be reiterated here.[17] Cross-correlation functions between two photons of the pump pulse and one photon of the probe pulse, measured independently, were invoked in the fit except that at 248.0 nm. At 248.0 nm, resonance-enhancement in the multiphoton ionization of Xe was observed which prevented a reliable determination of the cross-correlation between 2×248.0 and 332.9 nm. Therefore, the cross-correlation function at 244.2 nm was used in the fit of the TRPES data at 248.0 nm and it was varied in a small range to find a best fit (minimum χ^2 value). The photoelectron kinetic energy distribution(s) of component(s) involved at each pump wavelength, derived from the fit, are shown in Fig. 2(d)–(f). The energetic limit for ionization to the ground state of the cation (D_0), calculated using the previously reported ionization potential of 12.62 eV,[18] is indicated with a black arrow. The derived time constants for the $\tilde{C}$ electronic state are summarized in Table 1. The photoelectron transients over the kinetic energy range 1.0–1.2 eV where the main feature of the $\tilde{C}$ state is located (*vide infra*) are shown in Fig. 2(g)–(i), together with the curves from the 2D global fit. In the data analysis, time-zeros were varied in the range of the time-zero drift experimentally measured and the cross-correlations were also varied in the range of their uncertainties to obtain a best fit. This analysis also served to estimate the confidence intervals of these time constants.

At 248.0 nm, it is straight forward to assign the strong, single peak feature to the $\tilde{C}(000)$ vibronic state, with a lifetime of 1.42 $\pm$ 0.15 ps. The $\tilde{C}$ state is a Rydberg state with an electron from the highest occupied molecular orbital (HOMO) excited to the $3pa_1$ Rydberg orbital, and as such it may be expected to possess a minimum energy geometry very close to that of the D_0 state of the cation, resulting in the photoionization process being dominated by diagonal Franck–Condon (FC) factors ($\Delta\nu = 0$). In the present case, the $D_0(000)$ vibronic state of the cation is expected which is consistent with the observations in the photoelectron kinetic energy distribution: a single peak

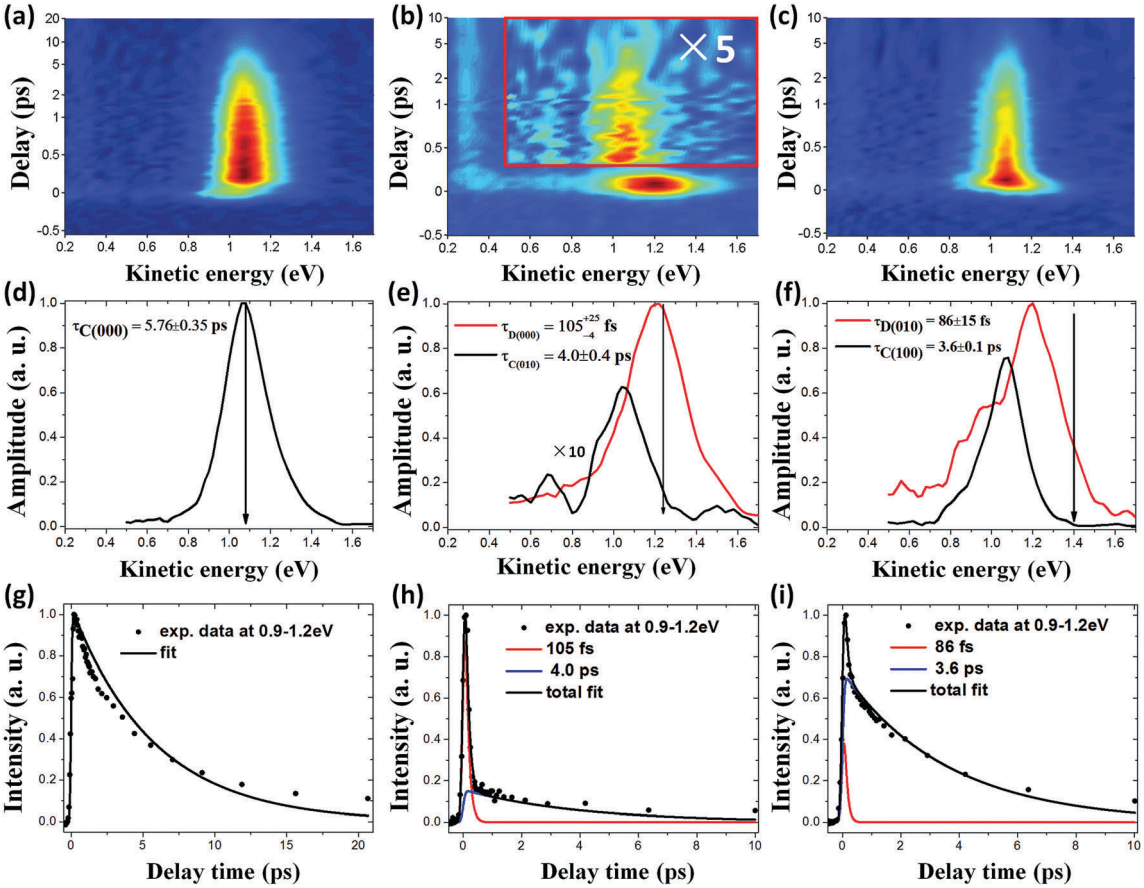

Fig. 3 Same as Fig. 2, but for D_2O at pump wavelengths of 248.0 (a), 244.2 (b) and 240.1 nm (c).

located at the energetic limit. At 244.2 nm, there are two components involved, with a lifetime of 327^{+23}_{-47} and 52^{+12}_{-6} fs, respectively. The fit also suggests that these two components have a parallel relationship, *i.e.*, these two components are excited simultaneously and decay independently. According to the assignment in the absorption spectrum, there are two vibronic states covered by the bandwidth of the 244.2 nm pump pulse ($\sim$400 cm^{-1}), $\tilde{D}(000)$ and $\tilde{C}(010)$, with the former having a much larger absorption cross section than the latter. Similar to the $\tilde{C}(000)$ TRPES data, the photoelectron from the $\tilde{D}(000)$ vibronic state should also correspond to a single peak at the energetic limit ($\tilde{D}$ is also a Rydberg state), *i.e.*, the 52 fs component corresponds to the $\tilde{D}(000)$ vibronic state. In the photoionization of the $\tilde{C}(010)$ vibronic state, the $\nu_2 = 1$ vibrational excitation will be conserved in the cation, leading to the formation of the $D_0(010)$ vibronic state of the cation, due to the $\Delta\nu = 0$ FC propensity in the photoionization step. Therefore, the photoelectrons from the $\tilde{C}(010)$ vibronic state will have the same kinetic energy as that from the $\tilde{C}(000)$ vibronic state when the same probe wavelength is used. This is indeed what was observed in the experiment (Fig. S1, ESI†), confirming that the other component corresponds to the $\tilde{C}(010)$ vibronic state, with a lifetime of 327^{+23}_{-47} fs. There is a negative dip in the kinetic energy distribution of the photoelectron of the $\tilde{C}(010)$ state. This is an artificial structure from the 2D global fit, due to the much strong neighboring peak in the photoelectron kinetic energy distribution of the $\tilde{D}(000)$ state. As for TRPES data at 239.0 nm, similar analysis was performed and the 643^{+160}_{-183} fs component is attributed to the $\tilde{C}(100)$ vibronic state. According to the absorption spectrum, the component with a lifetime less than 50 fs should be the $\tilde{D}(010)$ vibronic state. However, the corresponding photoelectron kinetic energy distribution is very diffuse, covering the whole range from 1.5 down to 0.2 eV, inconsistent with the expectation of the photoionization of the $\tilde{D}$ Rydberg state. Very likely, this is due to contamination from the non-resonant two-color multiphoton ionization. The very weak pump–probe signal and the short lifetime of the $\tilde{D}(010)$ state make it indistinguishable from the non-resonant background (it is therefore labelled as τ_{non} in Fig. 2(f)). The TRPES data for the D_2O molecule, shown in Fig. 3(a–c), are fitted and analyzed in an analogous manner and lifetimes of 5.76 ± 0.35, 4.0 ± 0.4 and 3.6 ± 0.1 ps are derived for the $\tilde{C}(000)$, $\tilde{C}(010)$ and $\tilde{C}(100)$ states, respectively.

The predissociation dynamics of water excited to the $\tilde{C}$ state and the vibrational excitation effects

The lifetimes of the $\tilde{C}(000)$ state derived in the current study are in reasonable agreement with the previous studies, but obvious differences also exist. By measuring the line width in the 3 + 1 REMPI spectra, Ashfold *et al.* estimated the upper limit for the

lifetime of the $\tilde{C}$ state.[5] They obtained 2.5 ps for H_2O and 6 ps for D_2O at the lowest rotational quantum number $\langle \hat{J}_a^2 = 0 \rangle$. In a time resolved study, Radloff and co-workers directly measured the lifetime of the $\tilde{C}$ state, leading to 0.5 ± 0.1 and 1.2 ± 0.1 ps for H_2O and D_2O, respectively.[8] The lifetimes derived from the current study are between the results from those two previous studies for both H_2O and D_2O. This might be due to the different rotational temperatures of the water samples used in these experiments. It was concluded that the lifetime of the $\tilde{C}$ state decreases rapidly with increasing rotational excitation of the water molecules, scaled with $\langle \hat{J}_a^2 \rangle$. The experiment of Radloff and co-workers was performed with water vapor at room temperature, and therefore a relatively high average $\langle \hat{J}_a^2 \rangle$ and a smaller (state averaged) lifetime are expected for both H_2O and D_2O. The current experiment was performed with a molecule beam, and therefore only a very small, but non-zero $\langle \hat{J}_a^2 \rangle$ is anticipated. Therefore, the lifetimes from the current experiment are larger than those from Radloff and co-workers, but smaller than ones for $\langle \hat{J}_a^2 = 0 \rangle$ derived by Ashfold *et al.* As such, the observed difference in the lifetimes of the $\tilde{C}(000)$ state for both H_2O and D_2O is due to the temperature difference of the water samples used in three experiments which in turn confirms the previous conclusion: the lifetime of the $\tilde{C}(000)$ state decreases rapidly with the increase of $\langle \hat{J}_a^2 \rangle$.

Besides the vibrational ground state, bending and symmetric stretching mode excited states of the $\tilde{C}$ electronic state were also accessed, enabling an investigation of vibrational excitation effects on the predissociation dynamics of the $\tilde{C}$ state. From Table 1, the vibrationally excited states all show faster predissociation. This might be due to the following two factors: (1) energetic factor: The vibrational excited states locate energetically higher than the vibrational ground state and higher densities of state of the $\tilde{A}$ and $\tilde{B}$ states are expected, resulting in faster predissociation rates (Fermi Golden Rules); (2) FC factor: Compared to the vibrational ground state, the structured wavefunction of the vibrationally excited states on the bound $\tilde{C}$ state potential energy surface (PES) might have a larger overlap integral with the outgoing wavefunction on the $\tilde{A}$ or $\tilde{B}$ state PES, which is highly oscillatory, resulting in a faster predissociation. In particular, the bending mode excited wavefunction should have a larger overlap with the outgoing wavefunction on the $\tilde{B}$ state PES which contains extensive nodes along the bending angle as shown by Dixon and coworkers.[9] Therefore, the $\tilde{C}(010)$ state should be more efficiently predissociated by the B state. As for the $\tilde{A}$ state, the outgoing wavefunction is highly oscillatory along the symmetric stretching coordinate and the $\tilde{C}(100)$ state should have a larger FC overlap with and is more easily predissociated by the $\tilde{A}$ state. Both energetic and FC factors might play a role in promoting the predissociation of the $\tilde{C}$ state. It is hard to separate the contributions of these factors solely from the current experimental data. High level theoretical work is definitely needed to examine these proposals and provide further details into vibrational excitation effects on the predissociation dynamics of the $\tilde{C}$ state of water.

From Table 1, the most remarkable observation is that the bending mode excitation of H_2O shows an "abnormal" enhancement in the predissociation rate of the $\tilde{C}$ state by a factor of about

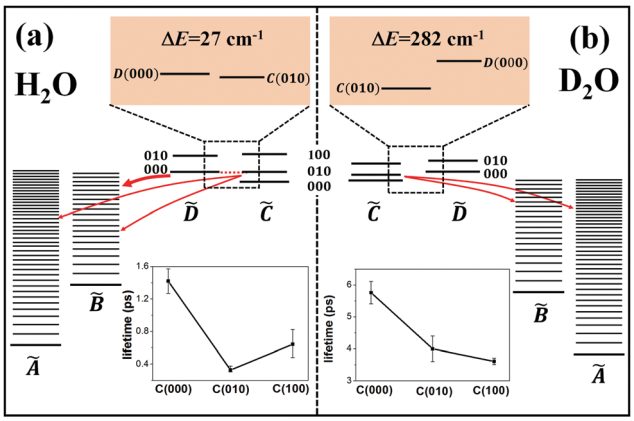

Fig. 4 Schematic view of the energy levels of water molecules for the related electronic states and the predissociation pathways of the $\tilde{C}$ state. The inset panels show the lifetimes of the $\tilde{C}$ state with different vibrational excitation.

4.3, with an additional vibrational energy of about 1400 cm^{-1}. The symmetric stretching excitation enhances the predissociation rate only by a factor of 2.2 with more than two times additional vibrational energy. While for D_2O, only a factor of 1.4 is observed in the predissociation rate enhancement in the $\tilde{C}$ state by the bending mode excitation. Therefore, it seems hard to rationalize the enhancement of the predissociation rate by the bending mode excitation in H_2O by only considering the two factors mentioned above and a third factor should play a role. A closer look at the vibronic levels of the $\tilde{C}$ state and the neighboring electronic states reveals that, as suggested by Ashfold *et al.* in their REMPI spectroscopy studies,[5,6] the state mixing between different vibronic levels has to be invoked. As shown in Fig. 4, the $\tilde{C}(010)$ and $\tilde{D}(000)$ vibronic states are isoenergetic and a strong wavefunction mixing is expected.[15] The latter is strongly predissociated by the $\tilde{B}$ state, with a lifetime of 52 fs (*vide supra*). This wavefunction mixing results in an additional predissociation pathway opening for the $\tilde{C}(010)$ state, besides the two well-known predissociation pathways *via* the $\tilde{A}$ or $\tilde{B}$ state: the $\tilde{C}(010)$ state predissociates through the $\tilde{D}$ state, followed by a fast decay of the latter to the $\tilde{B}$ state. The $\tilde{D}$ and $\tilde{B}$ states are strongly coupled at bent geometries.[19,20] The initial excitation in the bending mode of the $\tilde{C}(010)$ state might also facilitate the decay of the wavepacket on the $\tilde{D}$ state PES to the $\tilde{B}$ state. From the dramatic increase of the predissociation rate, the new predissociation pathway should play a dominant role in predissociation of the $\tilde{C}(010)$ state. Accordingly, the decay mechanism of the $\tilde{C}(010)$ state of H_2O is proposed as:

$$H_2O(\tilde{C}(010)) \xrightarrow{\text{accidental resonance}} H_2O(\tilde{D}(000)) \xrightarrow{\text{internal conversion}} H_2O(\tilde{B}) \quad \text{(major)},$$

$$H_2O(\tilde{C}(010)) \xrightarrow{\text{Coriolis coupling}} H_2O(\tilde{B}) \quad \text{(minor)},$$

$$H_2O(\tilde{C}(010)) \xrightarrow{\text{electronic coupling}} H_2O(\tilde{A}) \quad \text{(minor)},$$

$$H_2O(\tilde{B}) \xrightarrow{\text{conical intersection}} H_2O(\tilde{X}).$$

As such, the predissociation of H_2O in the $\tilde{C}(010)$ state provides an excellent example of competition between different non-adiabatic decay pathways with at least five electronic states involved. As for the $\tilde{C}(010)$ state of D_2O, there is a much larger energy gap (282 cm^{-1})[15] with the $\tilde{D}(000)$ state and therefore a negligible mixing between these two states exists and the predissociation of the $\tilde{C}(010)$ state of D_2O is barely affected.

Conclusions

In summary, the predissociation of water molecules in the electronic $\tilde{C}$ state was studied using the time-resolved photoelectron imaging method. The $\tilde{C}(000)$, $\tilde{C}(010)$ and $\tilde{C}(100)$ states of H_2O and D_2O were excited by two-photon absorption in the wavelength range of 248.0–239.0 nm. All these states were unambiguously identified in the time-resolved photoelectron spectra data and their lifetimes were measured. The derived lifetimes of the $\tilde{C}(000)$ state for both H_2O and D_2O are in reasonable agreement with previous experimental results, but with certain difference due to the different temperatures of the water samples used in various experiments. Finally, the vibrational excitation effects on the predissociation dynamics of water are discussed in detail. Vibrationally excited states all show faster predissociation which is attributed to the energetic and Franck–Condon factors. The bending mode excitation of H_2O shows an "abnormal" high enhancement in the predissociation rate with a factor of 4.3 which is rationalized by invoking an additional accidental resonance mediated pathway, highlighting a new decay mechanism of H_2O in the $\tilde{C}$ state.

Conflicts of interest

There are no conflicts to declare.

Acknowledgements

This work was supported by the National Natural Science Foundation of China (Grant No. 21573228), the Ministry of Science and Technology of China (2012YQ12004704) and the National Basic Research Program of China (973 Program, 2013CB922200). We would also like to thank Prof. Michael N. R. Ashfold for very helpful discussions.

References

1 R. Schinke, *Photodissociation dynamics*, Cambridge University Press, Cambridge, 1993.
2 B. P. Bonev, M. J. Mumma, M. A. DiSanti, N. Dello Russo, K. Magee-Sauer, R. S. Ellis and D. P. Stark, *Astrophys. J.*, 2006, **653**, 774.
3 B. P. Bonev and M. J. Mumma, *Astrophys. J.*, 2006, **653**, 788.
4 K. Yuan, R. N. Dixon and X. Yang, *Acc. Chem. Res.*, 2011, **44**, 369 and references therein.
5 M. N. R. Ashfold, J. M. Bayley and R. N. Dixon, *Chem. Phys.*, 1984, **84**, 35.
6 M. N. R. Ashfold, J. M. Bayley, R. N. Dixon and J. D. Prince, *Ber. Bunsenges. Phys. Chem.*, 1985, **89**, 254.
7 G. Meijer, J. J. Termeulen, P. Andresen and A. Bath, *J. Chem. Phys.*, 1986, **85**, 6914.
8 O. Steinkellner, F. Noack, H.-H. Ritze, W. Radloff and I. V. Hertel, *J. Chem. Phys.*, 2004, **121**, 1765.
9 K. Yuan, Y. Cheng, L. Cheng, Q. Guo, D. Dai, X. Wang, X. Yang and R. N. Dixon, *Proc. Natl. Acad. Sci. U. S. A.*, 2008, **105**, 19148.
10 K. J. Yuan, Y. A. Cheng, L. N. Cheng, Q. Guo, D. X. Dai, X. M. Yang and R. N. Dixon, *J. Chem. Phys.*, 2010, **133**, 134301.
11 Z. He, Z. Chen, D. Yang, D. Dai, G. Wu and X. Yang, *Chin. J. Chem. Phys.*, 2017, **30**, 247.
12 V. Dribinski, A. Ossadtchi, V. A. Mandelshtam and H. Reisler, *Rev. Sci. Instrum.*, 2002, **73**, 2634.
13 J. H. Fillion, R. van Harrevelt, J. Ruiz, N. Castillejo, A. H. Zanganeh, J. L. Lemaire, M. C. van Hemert and F. Rostas, *J. Phys. Chem. A*, 2001, **105**, 11414.
14 J. W. C. Johns, *Can. J. Phys.*, 1963, **41**, 209.
15 S. Bell, *J. Mol. Spectrosc.*, 1965, **16**, 205.
16 P. Gurtler, V. Saile and E. E. Koch, *Chem. Phys. Lett.*, 1977, **51**, 386.
17 G. R. Wu, A. E. Boguslavskiy, O. Schalk, M. S. Schuurman and A. Stolow, *J. Chem. Phys.*, 2011, **135**, 164309.
18 R. H. Page, R. J. Larkin, Y. R. Shen and Y. T. Lee, *J. Chem. Phys.*, 1988, **88**, 2249.
19 D. M. Hirst and M. S. Child, *Mol. Phys.*, 1992, **77**, 463.
20 R. van Harrevelt and M. C. van Hemert, *J. Chem. Phys.*, 2000, **112**, 5787.

